

Uncertainty-Aware Pedestrian Trajectory Prediction via Distributional Diffusion

Yao Liu^{1, *}Zesheng Ye^{1, *}Binghao Li²Lina Yao^{3,1}¹School of Computer Science and Engineering, University of New South Wales, Sydney, Australia.²School of Minerals and Energy Resources Engineering, University of New South Wales, Sydney, Australia.³Data 61, CSIRO, Sydney, Australia.

{yao.liu3, zesheng.ye, binghao.li, lina.yao}@unsw.edu.au

Abstract

Tremendous efforts have been devoted to pedestrian trajectory prediction using generative modeling for accommodating uncertainty and multi-modality in human behaviors. An individual's inherent uncertainty, e.g., change of destination, can be masked by complex patterns resulting from the movements of interacting pedestrians. However, latent variable-based generative models often entangle such uncertainty with complexity, leading to either limited expressivity or overconfident predictions. In this work, we propose to separately model these two factors by implicitly deriving a flexible distribution that describes complex pedestrians' movements, whereas incorporating predictive uncertainty of individuals with explicit density functions over their future locations. More specifically, we present an uncertainty-aware pedestrian trajectory prediction framework, parameterizing sufficient statistics for the distributions of locations that jointly comprise the multi-modal trajectories. We further estimate these parameters of interest by approximating a denoising process that progressively recovers pedestrian movements from noise. Unlike prior studies, we translate the predictive stochasticity to the explicit distribution, making it readily used to generate plausible future trajectories indicating individuals' self-uncertainty. Moreover, our framework is model-agnostic for compatibility with different neural network architectures. We empirically show the performance advantages of our framework on widely-used benchmarks, outperforming state-of-the-art in most scenes even with lighter backbones.

1. Introduction

Predicting human movements and pedestrian trajectories forms the cornerstone of safe autonomous human-machine interaction systems, such as intelligent transportation, urban planning, and underground mine automation [27, 50, 46].

*Yao Liu and Zesheng Ye are co-first authors with equal contributions.

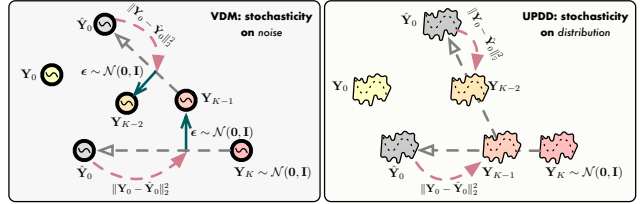


Figure 1. Illustrative difference between vanilla diffusion models (VDMs)¹ and UPDD. While VDMs rely on noises throughout the diffusion to introduce stochasticity, UPDD involves predictive uncertainty by modeling distributions rather than trajectories.

Large volumes of vehicles and crowded crossroads can easily pose a safety hazard to pedestrians; detecting and anticipating peoples' future movements may, however, reduce the risk significantly. Despite being valuable, this task is challenged by highly uncertain human behaviors resulting from interleaved self- and inter-pedestrian uncertainties. In one sense, while following the same historical path, two trajectories originating from one pedestrian can sometimes have different futures due to their different destinations. Meanwhile, pedestrians cannot ascertain each other's intentions and destinations but must uphold a certain amount of spatial separation, further amplifying the indeterminacy of the system. These uncertainties highlight the complex and multi-modal nature of human motion [14, 42].

In terms of complexity, trajectory prediction is viewed as a sequence-to-sequence task from a spatial-temporal viewpoint. In particular, the spatial correlation among pedestrians is attributed to the result of social factors [15, 1, 29]. For example, people also pay attention to not colliding with others while walking closely with companions sometimes. This motivates the use of increasingly powerful non-linear function approximators to represent such complex correlations when further taking into account temporal dependencies, most notably importance-weighted neighboring aggregation [45, 28, 14, 37] with Transformers [44] and dynamic social-temporal graphs [49, 19, 20, 38].

Upon this, it is now a standard practice to forecast multi-modal trajectories using generative models with latent variables [14], whereby the plausibility of future trajectories can hopefully be covered by a predictive distribution conditioned on a fixed historical context. By harnessing latent stochasticity, models predict the distribution (either explicitly or implicitly) of credible trajectories to approach the uncertainty. Specifically, the methods with explicit density functions for predictive distribution mostly rely on conditional variational autoencoders [26, 20, 38, 32, 5, 7] that assume Gaussian outputs. The trade-off results in latent representations with limited expressivity [4, 31, 43], often leading to unnatural generation [12]. Conversely, those implicit counterparts [14, 37, 51, 9] could benefit from more flexible generations without a fixed density form, thanks to the adoption of Generative Adversarial Networks (GANs) [11]. Still, training GANs has proven difficult to mitigate mode collapse [13, 35] and unstable gradients [21, 23]. Moreover, GANs sometimes make overconfident predictions [10], rendering difficulty in expressing predictive uncertainty. These latent variable models may struggle to balance expressivity with uncertainty since there is an inherent entanglement between multi-pedestrian complexity and self-uncertainty.

A recent bloom has been witnessed in denoising diffusion probabilistic models (i.e., diffusion models) [16] applied to image and text generation [36, 2]. Diffusion models draw inspiration from non-equilibrium thermodynamics that simulates particle diffusion by progressively injecting noise into data until the signal is destroyed. Then sampling high-fidelity data from random noise is achievable by learning to reverse such a diffusion process [40]. Intuitively, this setting lends itself well to modeling pedestrian motion. The movements of pedestrians within a system are determined by certain constraints, e.g., destinations and social regulations. Adding noise can therefore be viewed as discarding these constraints, resulting in more indeterminate human behaviors. In due course, the trajectories will become completely unpredictable once the system behaves like random noise. Of interest in trajectory prediction is the likelihood of trajectory density functions, though it is too complex to be derived directly. Alternatively, one can recover the true trajectory density function from a noisy system by approximating the reverse of the aforementioned diffusion process. In light of this, diffusion models were previously applied to trajectory prediction as attempted in vanilla diffusion models (VDMs). For instance, MID [12] assumes the indeterminacy of pedestrians' movements can be simulated by a Markovian diffusion process resembling our motivation. However, given that diffusion models limit the latent dimension to the input data, VDMs propose to generate the exact coordinates of every trajectory with a complete single

reverse process. When it comes to multi-modal predictions, this process has to be repeated multiple times with different sampled noises, not to mention that even generating an individual sample requires many iterations. In this sense, VDMs are inefficient for being much slower than previous approaches (e.g., roughly $\times 39$ slower than [38]).

Accordingly, we propose to explicitly parameterize the predictive distribution of trajectories rather than future trajectories themselves. As such, individuals' self-uncertainty can be separated from modeling complex multi-pedestrian movements. The key insight is to transform each pedestrian's exact trajectory into a readily sampled distribution, by assuming the bi-variate Gaussian form and computing their sufficient statistics. Then, we can operate the diffusion model with a joint parametric distribution over all pedestrians in future timesteps. By doing so, our approach transfers the predictive stochasticity from noises to the dedicated predictive distribution, allowing us to easily sample multiple trajectories and avoid running reverse diffusion intensively.

In more detail, our first step involves mapping ground-truth future trajectory data into sufficient statistics for a predictive trajectory distribution, using a neural network-based *Distribution Converter*. Following, we encode the historical and neighboring information of each pedestrian with a *guidance encoder*, providing guidance information [17] for a conditional diffusion model-based *trajectory generator*², an approximation of the true reverse diffusion. Moreover, concerning the efficiency issue, we follow [41] that relaxes the Markovian assumption of [16, 12] to accelerate sampling from noise, through the addition of multiple Markov jumps at once with deterministic transitions. Notably, a deterministic generative process like [41] inevitably challenges its use in MID to generate multi-modal predictions; on the other hand, our method leans stochasticity on the predictive distribution rather than sampling from noise. In summary, our contributions are:

- We present an Uncertainty-aware trajectory Prediction framework through Distributional Diffusion (UPDD). UPDD parameterizes the trajectory distribution by approximating reverse diffusion transitions that smoothly improve predictive confidence of future movements.
- We separate explicit uncertainty estimation of trajectories from complex motion prediction with denoising diffusion models. Our method generalizes previous diffusion model-based trajectory prediction approach to incorporate predictive uncertainty even with a single reverse outcome, enabling faster sampling with deterministically accelerated generative models.

¹The approaches (e.g., [12]) implementing diffusion models [16] directly on *trajectory* are termed vanilla diffusion models.

²There might be some ambiguity in the naming of *trajectory generator*. More precisely, we generate sufficient statistics, i.e., the distribution of trajectory, and then we sample trajectories therefrom.

- We demonstrate that our method empirically outperforms the state-of-the-art on real-world pedestrian trajectory prediction benchmarks. In addition, we show that the expressivity of a powerful generative framework is not overwhelmed by the complexity of integrated neural networks, thus suggesting design choices with smaller model sizes when efficiency is prioritized.

2. Related Work

Trajectory Forecasting as Spatial-temporal Prediction.

Often referred to as a sequence-to-sequence task, pedestrian trajectory forecasting uses historical trajectory data as input to predict the locations of multiple agents along future timesteps, taking their spatial correlations into account. This sequential nature makes autoregressive recurrent structures [18, 8] a fruitful option. Social-LSTM [1] is a pioneering work that incorporates social interactions between agents into a recurrent neural network (RNN) to capture both spatial and temporal dependencies. Later studies focus mainly on encoding dynamic influences from neighbors effectively. The attention-based methods [45, 28, 14, 37] aggregate neighboring information with different significance, while others construct a spatial-temporal graph to represent social interactions [49, 19, 20, 38]. Despite their popularity in sequential modeling, RNNs have been criticized for their inability to parallelize. This motivates the use of powerful Transformer [44] as an alternative. For instance, STAR [47] employs both temporal and spatial Transformers to capture complex spatial-temporal interactions in each dimension, respectively. In place of that, AgentFormer [48] proposes modeling two dimensions concurrently using a Transformer to prevent potential information loss caused by the independent encoding of either dimension. Even so, Transformers can sometimes pose challenges to model efficiency due to their parameter-intensive characteristics [39]. Instead, we discuss an alternative with both spatial and temporal convolutions toward a parameter-efficient solution of trajectory prediction. We empirically demonstrate that one can choose to use lightweight backbone networks, provided that a flexible generative framework is effectively employed.

Trajectory Forecasting as Conditional Generative Modeling.

Recent studies have embraced generative models to predict pedestrian trajectory distributions to account for uncertainty and multi-modality of future dynamics, conditioned on intermediate representations of historical trajectories. One can be categorized into either type depending on whether the model outputs an explicit predictive distribution. Centering around conditional variational autoencoders (cVAEs), the explicit models [26, 20, 38, 32, 5, 7] are learned by maximizing the likelihood of predictive distribution with concrete function form. As an example, [32, 5] assume the locations subject to a bi-variate Gaussian at each timestep. While the explicit function form allows for easier

sampling and optimization, it comes with a cost of limited expressivity and jagged trajectory generation [12]. The implicit generation [14, 37, 51, 9], on the other hand, is shown to be more flexible by following generative adversarial networks (GANs) [11]. Specifically, these methods generate trajectories from random noise and adopt a discriminator to distinguish those generated from the ground-truth. However, training GAN is notorious for being unstable, despite subsequent efforts to alleviate mode collapses, such as reversible transformations [19] and multiple generators [9]. Furthermore, the latest framework MID [12] sheds light on addressing the issues in both GANs and cVAEs worlds by leveraging diffusion models [16]. Similar to our motivation, MID regards the future trajectory as a whole and gradually reduces the prediction indeterminacy by learning to reverse a diffusion process that transforms a deterministic ground-truth trajectory into the stochastic Gaussian noise. As such, MID is easier to train than GAN-based approaches whilst producing more accurate predictions than cVAE-based counterparts. Nevertheless, MID predicts exact coordinates rather than a distribution. In this case, obtaining multiple plausible paths are time-consuming since each sample can only be obtained with a complete denoising process. Unlike MID, our method enforces a mixture of bi-variate Gaussian predictions per timestep, thus enabling faster sampling from the explicit density function while still handling complex patterns of multi-pedestrian movements.

3. Methodology

3.1. Problem Formulation

We consider the pedestrian trajectory prediction without auxiliary information, e.g., scene context and destination. Assume N pedestrians walking in a scene. Having observed their historical 2D locations $\mathbf{X} = \{\mathbf{x}^{(n)}\}_{n=1:N} \in \mathbb{R}^{N \times T \times 2}$ with $\mathbf{x}^{(n)} = \{\mathbf{x}_t^{(n)}\}_{t=1:T}$ throughout T timesteps, we generate multiple plausible trajectories for each pedestrian indicating future locations. As of all N pedestrians, we have the prediction $\hat{\mathbf{Y}} = \{\mathbf{y}^{(n)}\}_{n=1:N} \in \mathbb{R}^{N \times T' \times 2}$ in the next T' timesteps by parameterizing a conditional predictive distribution $p_\theta(\mathbf{Y}|\mathbf{X})$. Since $p_\theta(\mathbf{Y}|\mathbf{X})$ actually describes a joint outcome over $N \times T'$ variables, we can sample multiple predicted trajectories for any pedestrian therefrom.

3.2. Method Overview

As part of generative approaches, we aim to learn the true distribution of future trajectories $p(\mathbf{Y}|\mathbf{X})$ with a parametric approximation $p_\theta(\mathbf{Y}|\mathbf{X})$. For each pedestrian (indexed by n), let $p(\mathbf{y}_n^t | \mathbf{y}_n^{t-1}, \mathbf{X}) = \mathcal{N}(\mathbf{y}_n^t; \mu_1, \mu_2, \sigma_1, \sigma_2, \rho)$ be a bi-variate Gaussian distribution parameterized by its sufficient statistics, where $\mu_1, \mu_2, \sigma_1, \sigma_2$ are predictive means and standard deviations for each 2D coordinate, ρ measures the correlation between two dimensions. To capture com-

plex and multi-modal $p(\mathbf{Y}|\mathbf{X})$, we build our generative process upon flexible diffusion models, equipped with explicit density forms at each location³. Specifically, we estimate predictive sufficient statistics by parameterizing a reverse diffusion chain that starts from random noise and progressively reduces the uncertainty of possible future trajectories.

Fig. 2 overviews the proposed Uncertainty-Aware trajectory Prediction framework with Distributional Diffusion (UPDD). UPDD includes four trainable modules $\Theta := \{\phi, \psi, \varphi, \theta\}$. (a) *guidance information extractor* is applied to each pedestrian, encoding historical trajectory with $\phi(\cdot)$ and social information with $\psi(\cdot)$, respectively; (b) *distribution converter* $\varphi(\cdot)$ establishes a mapping from exact future trajectories to the parameters; (c) *trajectory generator* $\theta(\cdot)$ approximates the true denoising transition and parameterizes the distribution of future trajectory. These trainable modules are optimized jointly under a supervised paradigm.

3.3. Extracting Guidance Information

Commonsense says that pedestrians’ trajectories depend on their past movements and surroundings. To this end, we explore two pure CNN-based encoders $\phi(\cdot)$ and $\psi(\cdot)$ for extracting each pedestrian’s historical and neighboring information, respectively. Nonetheless, one can substitute them with any RNN-based (e.g., [14, 37]) or Transformer-based (e.g., [47, 48]) spatial-temporal encoders, since UPDD is essentially a model-agnostic probabilistic framework.

Encoding Historical Information. The raw trajectory data describes the relative coordinates of pedestrians. Generally, the historical encoder ϕ performs the following operations. For each pedestrian n with historical observations of T steps, we first apply a 1D-CNN with T kernels on the input features to calculate the influences of previous steps on the last (current) timestep. Given that $t = T$ is the most influential step for $t = T + 1$, we then concatenate the last timestep of the resulting T feature maps; and lastly adjust the importance of the concatenation using self-attention [44] to obtain the historical context encoding $\hat{\mathbf{x}}_\phi^{(n)}$.

Encoding Neighboring Influences. The neighboring effects are believed to be substantial for each pedestrian, typically referred to as social interaction information [1, 14, 37]. Thus, we design a neighbor encoder $\psi(\cdot)$ to encode all of the neighbors’ historical information for each pedestrian as well. As the number of neighbors may vary over time, we first aggregate the input features of neighbors for each timestep t , leading to T aggregated input features of pedestrian n . Accordingly, the subsequent operations are analogous to $\phi(\cdot)$ but handle the features of neighbors, eventually producing the neighboring context encoding $\hat{\mathbf{x}}_\psi^{(n)}$. We include more details of $\phi(\cdot)$ and $\psi(\cdot)$ in Appendix A.

³We only assume the bi-variate Gaussian density in each location, but not the concrete form of $p_\theta(\mathbf{Y}|\mathbf{X})$.

Having obtained both historical $\hat{\mathbf{x}}_\phi^{(n)}$ and neighboring information $\hat{\mathbf{x}}_\psi^{(n)}$, we concatenate them into pedestrian guidance information used in the generative model discussed in Sec. 3.5. In the following sections, we overload the term \mathbf{X} to denote the guidance information of all pedestrians and omit the subscript ϕ, ψ for clarity unless mentioned.

3.4. Mapping Trajectory to Sufficient Statistics

To preserve the predictive uncertainty of future trajectories, we map the exact trajectory data into sufficient statistics of the bi-variate Gaussian density function at each timestep, i.e., $\varphi : \mathbb{R}^{N \times T' \times 2} \rightarrow \mathbb{R}^{N \times T' \times 5}$. In other words, we aim to establish a deterministic non-linear transformation over all samples in the location space. Our implementation is a CNN here (can still be any other function approximators), such that

$$\mathbf{y}_{t,\varphi}^{(n)} = \varphi(\mathbf{y}_t^{(n)}), \text{ for } \forall n, \forall t \quad (1)$$

with $\mathbf{y}_{t,\varphi}^{(n)} := \{\mu_1, \mu_2, \sigma_1, \sigma_2, \rho\} \in \mathbb{R}^5$

Each of these 5D vectors determines each pedestrian’s approximated distribution and constitutes the joint event \mathbf{Y}_φ taking all pedestrians and timesteps into account.

3.5. Parameterizing Predictive Distribution

We now detail the diffusion process for reconstructing future trajectories over all pedestrians with the aforementioned sufficient statistics by considering them as “samples” in the generative model. We overload and slightly abuse the term \mathbf{Y}_0 to denote these samples for brevity. As discussed in [16], the diffusion process defines a K -iteration Markov chain $\{\mathbf{Y}_0, \dots, \mathbf{Y}_K|\mathbf{X}\}$ corrupting the samples \mathbf{Y}_0 to the noises \mathbf{Y}_K that span over the whole walkable area in our case. The diffusion chain is fixed to $q(\mathbf{Y}_{1:K}|\mathbf{Y}_0, \mathbf{X}) = \prod_{k=1}^K q(\mathbf{Y}_k|\mathbf{Y}_{k-1}, \mathbf{X})$ in an autoregressive manner, with each intermediate transition defined as a Gaussian, parameterized by strictly decreased $\alpha_{k-1} > \alpha_k \in (0, 1]$:

$$q(\mathbf{Y}_k|\mathbf{Y}_{k-1}, \mathbf{X}) = \mathcal{N}\left(\mathbf{Y}_k|\mathbf{X}; \sqrt{\frac{\alpha_k}{\alpha_{k-1}}} \mathbf{Y}_{k-1}, \left(1 - \frac{\alpha_k}{\alpha_{k-1}}\right) \mathbf{I}\right) \quad (2)$$

Notably, we can directly compute a closed-form final state \mathbf{Y}_K using input \mathbf{Y}_0 , enabled by recursive sampling with the reparameterization trick [22] in Gaussian transitions,

$$q(\mathbf{Y}_K|\mathbf{Y}_0, \mathbf{X}) = \int q(\mathbf{Y}_{1:K}|\mathbf{Y}_0, \mathbf{X}) d\mathbf{Y}_{1:K-1} \quad (3)$$

$$= \mathcal{N}(\mathbf{Y}_K|\mathbf{X}; \sqrt{\alpha_K} \mathbf{Y}_0, (1 - \alpha_K) \mathbf{I})$$

That is, by sequentially adding noise to \mathbf{Y}_0 , the forward diffusion eventually converts it into a standard Gaussian noise \mathbf{Y}_K when α_K is sufficiently close to 0. Learning to reverse the forward process allows us to recover input samples from

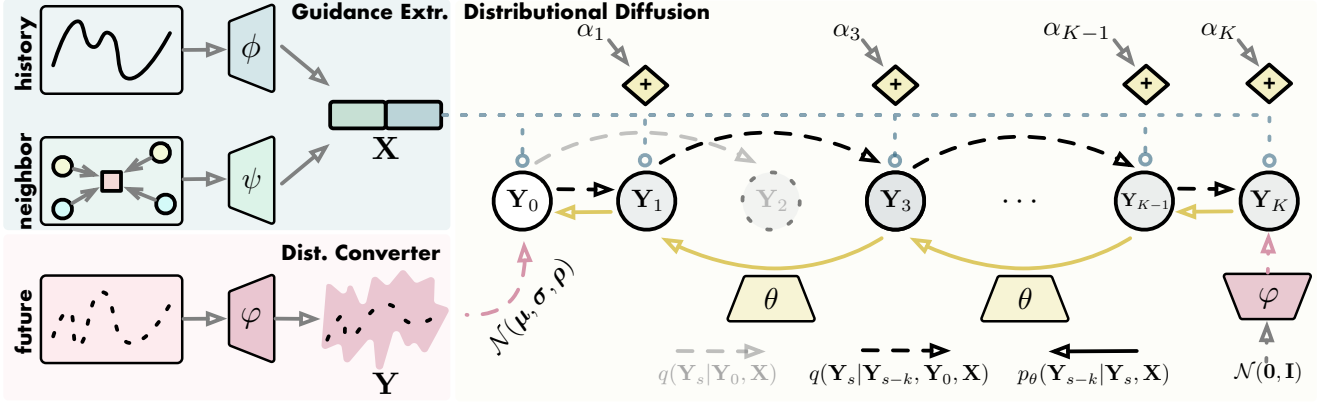


Figure 2. The overview of UPDD, consisting of *guidance extractor* (in Sec. 3.3), *distribution converter* (in Sec. 3.4) and *distributional diffusion* (in Sec. 3.5). To account for multi-modal human movements, UPDD approximates the distributions of future trajectories under a diffusion model-based generative framework. We encode historic and neighboring effects for each pedestrian to guide conditional diffusion; we map future trajectories into sufficient statistics of a parametric distribution approximating the true distribution, enabling fast sampling of future trajectories therefrom; we also speed up the generation with a non-Markovian “diffusion” chain by skipping certain steps.

noise. With the guidance information extracted from historical observations \mathbf{X} , we thus have the conditional generation process by marginalizing all the intermediate variables,

$$\begin{aligned} p_\theta(\mathbf{Y}_0|\mathbf{X}) &= \int p_\theta(\mathbf{Y}_{0:K}|\mathbf{X}) d\mathbf{Y}_{1:K} \\ &= \int p_\theta(\mathbf{Y}_K) \prod_{k=1}^K p_\theta(\mathbf{Y}_{k-1}|\mathbf{Y}_k, \mathbf{X}) d\mathbf{Y}_{1:K} \quad (4) \end{aligned}$$

with $p_\theta(\mathbf{Y}_K) = \mathcal{N}(\mathbf{0}, \mathbf{I})$.

where the parameters of θ are shared throughout the reverse chain, implemented as *trajectory generator*. Since the true reverse process $q(\mathbf{Y}_{k-1}|\mathbf{Y}_k, \mathbf{X})$ is generally intractable, we optimize a variational lower bound under instead:

$$\begin{aligned} &\max_{\theta} \mathbb{E}_{p(\mathbf{Y}_0|\mathbf{X})} [\log p_\theta(\mathbf{Y}_0|\mathbf{X})] \\ &\geq \max_{\theta} \mathbb{E}_{p(\mathbf{Y}_0, \mathbf{Y}_1, \dots, \mathbf{Y}_K|\mathbf{X})} \left[\log \frac{p_\theta(\mathbf{Y}_{0:K}|\mathbf{X})}{q(\mathbf{Y}_{1:K}|\mathbf{Y}_0, \mathbf{X})} \right] \\ &= \max_{\theta} \mathbb{E}_{p(\mathbf{Y}_0, \mathbf{Y}_1, \dots, \mathbf{Y}_K|\mathbf{X})} \left[\log p_\theta(\mathbf{Y}_K) - \sum_{k=1}^K \log \frac{p_\theta(\mathbf{Y}_{k-1}|\mathbf{Y}_k, \mathbf{X})}{q(\mathbf{Y}_K|\mathbf{Y}_{k-1}, \mathbf{X})} \right] \quad (5) \end{aligned}$$

where the true distribution is termed by $p(\mathbf{Y}_0|\mathbf{X})$ to be fitted with $p_\theta(\mathbf{Y}_0|\mathbf{X})$. Empirically, Eq. 5 can be simplified to the mean squared error between the “predicted” noise added to the sample and a noise ϵ_k randomly drawn from a standard diagonal Gaussian throughout K steps,

$$\begin{aligned} \min_{\theta} \mathcal{L}_{\text{emp}} &= \sum_{k=1}^K \mathbb{E}_{\mathbf{Y}_0 \sim p(\mathbf{Y}_0|\mathbf{X}), \epsilon_k \sim \mathcal{N}(\mathbf{0}, \mathbf{I})} [\|\theta(\hat{\epsilon}_k) - \epsilon_k\|_2^2] \quad (6) \\ &\text{with } \hat{\epsilon}_k = \sqrt{\alpha_k} \mathbf{Y}_0 + \sqrt{1 - \alpha_k} \epsilon_k \end{aligned}$$

when we sample \mathbf{Y}_k by applying the reparameterization trick on $q(\mathbf{Y}_k|\mathbf{Y}_0, \mathbf{X})$ each step⁴.

Moreover, we can follow [41] that potentially “shorten” the Markovian diffusion process by adding certain Markov jumps simultaneously, as a way to accelerate sampling from diffusion models with a similar surrogate objective.

Non-Markovian Forward Process. Observing a large K in Eq. 3 introduces a trade-off between how close $p(\mathbf{Y}_K)$ gets to a standard Gaussian [40] and the running efficiency of autoregressive sampling, we adopt a non-Markovian forward process that generalizes a Markovian diffusion while maintaining Gaussianity in Eq. 3. Consider a forward process where the transition also depends on \mathbf{Y}_0 , we have its joint distribution as,

$$\begin{aligned} q_\gamma(\mathbf{Y}_{1:K}|\mathbf{Y}_0, \mathbf{X}) &= q_\gamma(\mathbf{Y}_K|\mathbf{Y}_0, \mathbf{X}) \prod_{k=2}^K q_\gamma(\mathbf{Y}_{k-1}|\mathbf{Y}_k, \mathbf{Y}_0, \mathbf{X}) \quad (7) \end{aligned}$$

To ensure Gaussianity in each intermediate state depending on \mathbf{Y}_0 , such that

$$q_\gamma(\mathbf{Y}_k|\mathbf{Y}_0, \mathbf{X}) = \mathcal{N}(\mathbf{Y}_k|\mathbf{X}; \sqrt{\alpha_k} \mathbf{Y}_0, (1 - \alpha_k) \mathbf{I}) \quad (8)$$

for all $k > 0$, we define the true reverse transition as

$$\begin{aligned} q_\gamma(\mathbf{Y}_{k-1}|\mathbf{Y}_k, \mathbf{Y}_0, \mathbf{X}) &= \mathcal{N} \left(\sqrt{\alpha_{k-1}} \mathbf{Y}_0 + \sqrt{1 - \alpha_{k-1} - \gamma_k^2} \frac{\mathbf{Y}_k - \sqrt{\alpha_k} \mathbf{Y}_0}{\sqrt{1 - \alpha_k}}, \gamma_k^2 \mathbf{I} \right) \quad (9) \end{aligned}$$

where $\gamma \in \mathbb{R}^K$ controls the stochasticity added to each step. That is, the transition becomes deterministic if $\gamma \rightarrow 0$. Resembling Eq. 5, the variational lower bound is empirically

⁴While Eq. 5 and Eq. 6 are designed for θ , the variables \mathbf{Y}_0 and \mathbf{X} are parameterized by φ and ϕ, ψ , so they are jointly optimized.

approximated by,

$$\begin{aligned} & \max_{\theta} \mathbb{E}_{q_{\gamma}(\mathbf{Y}_{0:T})} \left[\log \frac{p_{\theta}(\mathbf{Y}_{0:K}|\mathbf{X})}{q_{\gamma}(\mathbf{Y}_{1:K}|\mathbf{Y}_0, \mathbf{X})} \right] \\ &= \mathbb{E}_{q_{\gamma}(\mathbf{Y}_{0:T})} \left[\log p_{\theta}(\mathbf{Y}_K) + \sum_{k=1}^K \log p_{\theta}(\mathbf{Y}_{k-1}|\mathbf{Y}_k, \mathbf{X}) \right. \\ & \quad \left. - \log q_{\gamma}(\mathbf{Y}_K|\mathbf{Y}_0, \mathbf{X}) - \sum_{k=2}^K (q_{\gamma}(\mathbf{Y}_{k-1}|\mathbf{Y}_k, \mathbf{Y}_0, \mathbf{X})) \right] \end{aligned} \quad (10)$$

where $\log p_{\theta}(\mathbf{Y}_{k-1}|\mathbf{Y}_k, \mathbf{X})$ approximates the true denoising step and is parameterized by our *trajectory generator*, whereas the other three terms have been derived previously. Still, the gradients are calculated with respect to the mean square error as in Eq. 6. More precisely, the generation starts from noise $p_{\theta}(\mathbf{Y}_K) = \mathcal{N}(0, \mathbf{I})$ and sequentially parameterizes next transition by replacing \mathbf{Y}_0 in Eq. 9:

$$\begin{aligned} & p_{\theta}(\mathbf{Y}_{k-1}|\mathbf{Y}_k, \mathbf{X}) \\ &= q_{\gamma} \left(\mathbf{Y}_{k-1}|\mathbf{Y}_k, \frac{\mathbf{Y}_k - \sqrt{1 - \alpha_k} \cdot \theta(\mathbf{Y}_k|\mathbf{X})}{\sqrt{\alpha_k}} \right) \end{aligned} \quad (11)$$

where $\theta(\mathbf{Y}_k|\mathbf{X})$ is our *trajectory generator* conditioned on guide information \mathbf{X} . See details of $\theta(\cdot)$ in Appendix A.

Accelerated Deterministic Reverse Process. As we have shown, a non-Markovian forward process that conditions each intermediate step on \mathbf{Y}_0 allows us to express the joint $q_{\gamma}(\mathbf{Y}_{0:T}|\mathbf{Y}_0)$ in a flexible way, so long as the Gaussianity in $q_{\gamma}(\mathbf{Y}_t|\mathbf{Y}_0)$ for all $t > 0$ is ensured. Intuitively, this implies reducing the number of iterations with another forward process fulfilling such requirements. Specifically, we can arbitrarily sample a sub-sequence $\tau \subset \{1, \dots, K\}$ (with length $S < T$) to form a forward process with $q_{\gamma}(\mathbf{Y}_{\tau_i}|\mathbf{Y}_0) = \mathcal{N}(\mathbf{Y}_{\tau_i}; \sqrt{\alpha_{\tau_i}}\mathbf{Y}_0, \sqrt{1 - \alpha_{\tau_i}}\mathbf{I})$. As such, the joint distribution can be factorized into

$$\begin{aligned} & q_{\gamma}(\mathbf{Y}_{1:K}|\mathbf{Y}_0) \\ &= q_{\gamma}(\mathbf{Y}_{\tau_S}|\mathbf{Y}_0) \prod_{i \in \tau_S} q_{\gamma}(\mathbf{Y}_{\tau_{i-1}}|\mathbf{Y}_{\tau_i}, \mathbf{Y}_0) \prod_{j \in \bar{\tau}} q_{\gamma}(\mathbf{Y}_j|\mathbf{Y}_0). \end{aligned} \quad (12)$$

where $\bar{\tau}$ involves steps not included in τ , thereby decreasing the required steps of forward iterations from K to S . Reversely, the generative process is also shortened to S steps. Having derived each term's closed form in Sec. 3.5, we can optimize the reverse process defined by Eq. 12 with Eq. 10. Further, upon sampling the noise $\mathbf{Y}_S \sim p_{\theta}(\mathbf{Y}_S)$, we get a deterministic generative process by setting $\gamma = 0$, proven to be more semantically meaningful in the latent space [41].

3.6. Sampling from Predictive Distribution

From $p(\mathbf{Y}_S)$, one can generate $\hat{\mathbf{Y}}_0$ by running the approximate reverse transition $p_{\theta}(\mathbf{Y}_{k-1}|\mathbf{Y}_k, \mathbf{X})$ iteratively. Recall that we parameterize the explicit density function of all pedestrians at each future timestep, i.e., $\hat{\mathbf{Y}}_0$ being sufficient statistics of the multi-modal predictions. For any

pedestrian n , the future trajectory can be generated by sampling from $p_{\theta}(\mathbf{Y}_0|\mathbf{X})$ throughout every future timestep as

$$\hat{\mathbf{y}}_t^{(n)} := (\hat{\mu}_{t,1}^{(n)}, \hat{\mu}_{t,2}^{(n)}) \sim \mathcal{N}(\mu_{t,1}^{(n)}, \mu_{t,2}^{(n)}, \sigma_{t,1}^{(n)}, \sigma_{t,2}^{(n)}, \rho_t^{(n)}) \quad (13)$$

for all $n \in [1, N]$ and $T < t < T'$. In this way, we can further easily sample trajectory predictions *as much as we want* from even with a single reverse run.

3.7. Multi-task Optimization

In addition to Eq. 10, we place two optimization objectives to account for the multi-modal nature of trajectories, and the consistency of predicted trajectories, respectively. One, we maximize the log-likelihood of ground-truth future trajectories \mathbf{Y} w.r.t the predictive bi-variate Gaussian parameterized by \mathbf{Y}_{φ} , towards an improved interpretation of true trajectories,

$$\min_{\Theta} \mathcal{L}_{\text{llh}} = - \sum_{n=1}^N \sum_{t=T+1}^{T'} \log(\mathbf{y}_t^{(n)}; \mathbf{y}_{t,\varphi}^{(n)}) \quad (14)$$

Second, to ensure that each predictive bi-variate Gaussian matches the correct exact location, we preserve their consistencies by minimizing the mean squared error as

$$\min_{\Theta} \mathcal{L}_{\text{con}} = \sum_{n=1}^N \|\mathbf{y}_{T+1}^{(n)} - \boldsymbol{\mu}_{T+1}^{(n)}\|_2^2. \quad (15)$$

where $\boldsymbol{\mu}_{T+1}^{(n)}$ are predictive means of $\mathbf{y}_{\varphi}^{(n)}$ at the first step of predictions, i.e., $t = T + 1$. We then express the overall training objective as a linear combination of Eq. 10, Eq. 14 and Eq. 15 with trade-off parameters λ_1, λ_2 and λ_3 .

4. Experiments and Analysis

4.1. Experiment Setup

Datasets. Our empirical evaluations are based on the ETH/UCY [34, 25] benchmarks, a widely-studied real-world trajectory prediction dataset consisting of five scenes: ETH, HOTEL, UNIV, ZARA1, ZARA2. Pedestrians in open areas are positioned in world coordinates for all scenes. Following common settings [38], we sample pedestrian movements every 0.4 seconds within each 8-second long video and convert the world coordinates to relative coordinates. Having observed the first 8 frames (3.2 seconds), prediction models are tasked with estimating pedestrian coordinates for the upcoming 12 frames (4.8 seconds).

Baselines. We compare UPDD with a range of state-of-the-art trajectory prediction approaches. Other than the deterministic approaches SocialLSTM [1] and STT [33], the rest include models with implicit density functions: SocialGAN [14], SoPhie [37], Social-BIGAT [24], MG-GAN [9], as well as the explicit ones: Trajectron++ [38], S-STGCNN [32], C-STGCNN [6], N-STGCNN [29] and DMRCNN [3]. Notably, MID [12] also employs a diffusion

Method	N	ETH	HOTEL	UNIV	ZARA1	ZARA2	AVG
SocialLSTM [1]	20	1.09/2.94	0.86/1.91	0.61/1.31	0.41/0.88	0.52/1.11	0.70/1.52
STT [33]	20	0.54/1.10	0.24/0.46	0.57/1.15	0.45/0.94	0.36/0.77	0.43/0.88
SocialGAN [14]	20	0.81/1.52	0.72/1.61	0.60/1.26	0.34/0.69	0.42/0.84	0.58/1.18
SoPhie [37] [†]	20	0.70/1.43	0.76/1.67	0.54/1.24	0.30/0.63	0.38/0.78	0.54/1.15
Social-BIGAT [24] [†]	20	0.69/1.29	0.49/1.01	0.55/1.32	0.30/0.62	0.36/0.75	0.48/1.00
MG-GAN [9] [†]	20	0.47/0.91	0.14/0.24	0.54/1.07	0.36/0.73	0.29/0.60	0.36/0.71
Trajectron++* [38]	20	0.67/1.18	0.18/0.28	0.30/0.54	<u>0.25/0.41</u>	0.18/0.32	0.32/0.55
S-STGCNN [32]	20	0.64/1.11	0.49/0.85	0.44/0.79	0.34/0.53	0.30/0.48	0.44/0.75
C-STGCNN [6]	20	0.64/1.00	0.38/0.45	0.49/0.81	0.34/0.53	0.32/0.49	0.43/0.66
N-STGCNN [29]	20	0.66/1.22	0.44/0.68	0.47/0.88	0.33/0.52	0.29/0.48	0.44/0.76
DMRCN [3]	20	0.60/1.09	0.21/0.30	0.35/0.63	0.29/0.47	0.25/0.41	0.34/0.58
STAR [47]	20	0.36/0.65	0.17/0.36	0.26/0.55	0.22/0.46	0.31/0.62	0.26/0.53
PECNet [30]	20	0.54/0.87	0.18/0.24	0.35/0.60	0.22/0.39	0.17/0.30	0.29/0.48
MID* [12]	20	0.54/0.82	0.20/0.31	0.30/0.57	0.27/0.46	<u>0.20/0.37</u>	0.30/0.51
UPDD(10/100)	10+10	0.40/0.82	0.22/0.43	<u>0.24/0.49</u>	0.31/0.64	0.25/0.50	<u>0.28/0.58</u>
UPDD(100/200)	10+10	<u>0.41/0.86</u>	<u>0.19/0.36</u>	0.23/0.49	0.23/0.49	0.21/0.43	0.25/0.53

Table 1. Overall quantitative comparisons with baselines in terms of ADE/FDE results (meters). [†] indicates models use auxiliary image information of scene context. * indicates a correction of results caused by the leakage of future paths. STAR and PECNet are not included for a fair comparison because they use different settings. We **bolded** the best results, while underlining the second best in each scene.

model for trajectory prediction comparable to UPDD. More details of baselines are outlined in Appendix B.

Metrics. We report Average Displacement Error (ADE) and Final Displacement Error (FDE) for quantitative evaluation as per most studies. ADE computes the average predictive error between the best estimation and the ground-truth trajectory. FDE measures the displacement error at the last point. We follow the leave-one-out evaluation criteria as in [38]: training on four out of five scenes and testing on the remaining scene. We report the Best-of-N result.

4.2. Comparison with State-of-the-Arts

Quantitative Evaluation. Tab. 1 compares UPDD with state-of-the-art in terms of ADE and FDE. We include two diffusion schemes with UPDD, in the form of S/K indicating execution steps and lengths of Markovian diffusion, respectively. Given the hybrid nature of UPDD, we sample credible trajectories in a 10+10 manner, i.e., run reverse diffusion 10 times, select the “best” prediction based on the predictive means in φ , and then sample 10 multi-modal trajectories therefrom with the explicit Gaussian density. Observe that UPDD in both schemes consistently demonstrates promising performances with ETH, UNIV and AVG results⁵. Generated approaches are generally advantageous provided they output multi-modal predictions. Moreover, both diffusion model-based approaches, MID and UPDD

reports the lowest AVG errors among all approaches, showing improved expressiveness thanks to the flexible diffusion models. Nevertheless, UPDD consistently outperforms MID apart from ZARA2.

Qualitative Results. In addition, we showcase visual comparisons of UPDD and MID with respect to the ground-truth trajectory as in Fig. 3. In most scenes, the best output of UPDD appears to successfully identify and follow the underlying pattern of data, while MID’s predictions generally stray more from the ground-truth.

Efficiency. Despite the great potential in learning complex data distribution, diffusion models are notoriously costly because it often takes hundreds or even thousands of reverse transitions to approach the data distribution from standard Gaussian noises. To address such a significant limitation of diffusion model-based approaches, we present an effective workaround for adapting deterministically accelerated “diffusion” models [41] to trajectory prediction. Upon comparing both the time and space complexity, we observe that UPDD is only with 40% parameters than that of MID and enjoys $3\times$ decreases in FLOPs with 1 iteration. Notably, while UPDD can benefit from the boost in speed, it is not the case for MID. Although both use diffusion models, UPDD parameterizes the explicit density functions for future locations whereas MID predicts the exact coordinates. This being the case, MID leans all its predictive stochasticity (for multi-modal generations) on sampled noises along with reverse diffusion, leaving it incompatible with deterministic acceleration. On the other hand, UPDD can (theoretically) abandon noise-induced randomness from each reverse transition, since the explicit predictive distribution naturally caters to the self-uncertainty of pedestrians. Moreover, the time complexity can be accentuated by the fact

⁵The original results of both Trajectron++ [38] and MID [12] are obtained upon leaked information <https://github.com/StanfordASL/Trajectron-plus-plus/issues/53>; we report the corrected results reproduced by the community and ourselves. STAR [47] and PECNet [30] sample trajectories per 0.24 seconds. Their prediction horizons are also shortened, making their results unfair to be involved in our comparison.

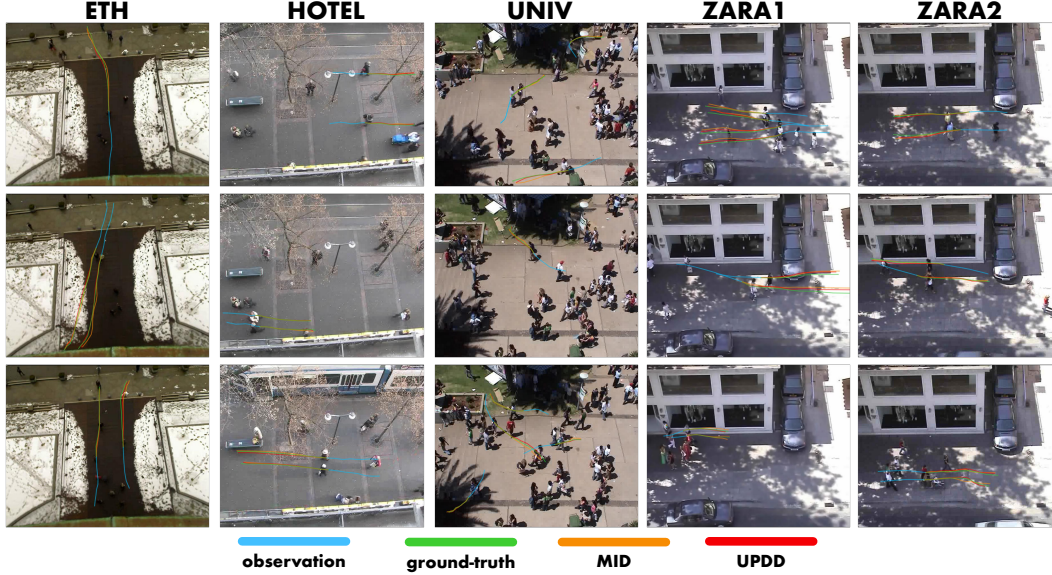


Figure 3. Qualitative Visualization

Variant	Steps	ADE/FDE
UPDD(I)	10/100	0.24/0.49
UPDD(I)	100/100	0.25/0.49
UPDD(I)	100/200	0.23/0.49
UPDD(I)	100/300	0.23/0.50
UPDD(P)	10	0.36/0.66
UPDD(P)	100	0.26/0.51

Table 2. Ablation with diffusion steps, with # of samplings fixed to 10+10.

Variant	Sample	ADE/FDE
A	10+10	0.23/0.49
B	20/1	0.34/0.77
C	1/20	0.41/0.79

Table 3. Ablation with different sampling strategies, retaining all other factors the same.

that the reverse diffusion must run many iterations, e.g., 100 steps for MID. Thus, the complexity scales linearly with the actual steps of execution, further emphasizing the benefits of shortening the reverse chain.

4.3. Ablation Studies

Diffusion Steps. We now discuss the effects of varying hyperparameters of the diffusion model in Tab. 2. We include variants with different total diffusion steps $K = 100, 200, 300$, but share the same execution steps $S = 100$. We find that changes in K do not seem to significantly affect the predictive performance; thus, a suitable ratio for shortening the chain may be chosen gently. We also showcase a variant with $K = 100$ and $S = 10$, which considerably slashes the generation time, while still remaining effective. Thus, one may consider this configuration if efficiency is of paramount importance. In addition, we replace the deterministically accelerated diffusion model in UPDD with the stochastic DDPM [16] used in MID, denoted by UPDD(P). In the case of $K = 10$, UPDD(P) may suffer from incom-

plete diffusion, leading to a performance gap with other competitors. The performance of UPDD(P) almost catches up with UPDD(I) when extending K to 100. The results suggest that UPDD naturally fits with deterministic “diffusion” chains since the stochasticity has been transferred to the predictive distribution, thereby no longer relying on noise sampling throughout the diffusion.

Hybrid Sampling. Tab. 3 shows our exploration of how UPDD is affected by different sampling strategies. Variant A refers to the standard UPDD, where we first run the reverse diffusion process 10 times and choose a “best” diffusion outcome (sufficient statistics of the trajectory distribution) with respect to the predictive means. We then sample 10 trajectories therefrom. In variant B, reverse diffusion is run 20 times with one trajectory sampled from each outcome, resembling MID. In variant C, a single run of reverse diffusion is conducted, but 20 trajectory samples are taken. In this sense, B attributes all stochasticity to random noise throughout the diffusion, disregarding the self-uncertainty in terms of the Gaussian predictions. Conversely, C may deteriorate due to a random sample given by the starting point of reverse diffusion (it only randomly samples a Gaussian noise once). It appears that both samplings degrade model performance, suggesting that the diffusion model becomes more effective when combined with Gaussian predictive distributions.

5. Conclusion and Outlook

We have presented an Uncertainty-aware Trajectory Prediction framework with distributional diffusion, which simulates the complex pedestrians’ movements with a flexi-

ble diffusion model, and predicts uncertain future locations with explicit bi-variate Gaussian distributions, respectively. While the distributional diffusion approximates the true denoising process that steadily improves confidence about future movement, the explicit predictive distributions of locations preserve inherent individual uncertainty that should not be eliminated. By doing so, we can even bypass expensive sampling of diffusion models with deterministic accelerated means which previous models cannot.

Limitation. UPDD requires careful choices for hybrid sampling with both diffusion and bi-variate Gaussian. While sampling from the explicit Gaussian can accelerate the process, the quality of generations depends on the outcome of reverse diffusion. It is worth exploring how to strike the right balance between efficiency and effectiveness.

References

- [1] Alexandre Alahi, Kratarth Goel, Vignesh Ramanathan, Alexandre Robicquet, Li Fei-Fei, and Silvio Savarese. Social lstm: Human trajectory prediction in crowded spaces. In *Proceedings of the IEEE conference on computer vision and pattern recognition*, pages 961–971, 2016. [1](#), [3](#), [4](#), [6](#), [7](#)
- [2] Jacob Austin, Daniel D Johnson, Jonathan Ho, Daniel Tarlow, and Rianne van den Berg. Structured denoising diffusion models in discrete state-spaces. *Advances in Neural Information Processing Systems*, 34:17981–17993, 2021. [2](#)
- [3] Inhwon Bae and Hae-Gon Jeon. Disentangled multi-relational graph convolutional network for pedestrian trajectory prediction. In *Proceedings of the AAAI Conference on Artificial Intelligence*, volume 35, pages 911–919, 2021. [6](#), [7](#)
- [4] Yuri Burda, Roger Grosse, and Ruslan Salakhutdinov. Importance weighted autoencoders. *arXiv preprint arXiv:1509.00519*, 2015. [2](#)
- [5] Yuning Chai, Benjamin Sapp, Mayank Bansal, and Dragomir Anguelov. Multipath: Multiple probabilistic anchor trajectory hypotheses for behavior prediction. *arXiv preprint arXiv:1910.05449*, 2019. [2](#), [3](#)
- [6] Guangyi Chen, Junlong Li, Jiwen Lu, and Jie Zhou. Human trajectory prediction via counterfactual analysis. In *Proceedings of the IEEE/CVF International Conference on Computer Vision*, pages 9824–9833, 2021. [6](#), [7](#)
- [7] Guangyi Chen, Junlong Li, Nuoxing Zhou, Liangliang Ren, and Jiwen Lu. Personalized trajectory prediction via distribution discrimination. In *Proceedings of the IEEE/CVF International Conference on Computer Vision*, pages 15580–15589, 2021. [2](#), [3](#)
- [8] Junyoung Chung, Caglar Gulcehre, KyungHyun Cho, and Yoshua Bengio. Empirical evaluation of gated recurrent neural networks on sequence modeling. *arXiv preprint arXiv:1412.3555*, 2014. [3](#)
- [9] Patrick Dendorfer, Sven Elfle, and Laura Leal-Taixé. Mgan: A multi-generator model preventing out-of-distribution samples in pedestrian trajectory prediction. In *Proceedings of the IEEE/CVF International Conference on Computer Vision*, pages 13158–13167, 2021. [2](#), [3](#), [6](#), [7](#)
- [10] Jakob Gawlikowski, Cedric Rovile Njietcheu Tassi, Mohsin Ali, Jongseok Lee, Matthias Humt, Jianxiang Feng, Anna Kruspe, Rudolph Triebel, Peter Jung, Ribana Roscher, et al. A survey of uncertainty in deep neural networks. *arXiv preprint arXiv:2107.03342*, 2021. [2](#)
- [11] Ian Goodfellow, Jean Pouget-Abadie, Mehdi Mirza, Bing Xu, David Warde-Farley, Sherjil Ozair, Aaron Courville, and Yoshua Bengio. Generative adversarial networks. *Communications of the ACM*, 63(11):139–144, 2020. [2](#), [3](#)
- [12] Tianpei Gu, Guangyi Chen, Junlong Li, Chunze Lin, Yongming Rao, Jie Zhou, and Jiwen Lu. Stochastic trajectory prediction via motion indeterminacy diffusion. In *Proceedings of the IEEE/CVF Conference on Computer Vision and Pattern Recognition*, pages 17113–17122, 2022. [2](#), [3](#), [6](#), [7](#)
- [13] Ishaan Gulrajani, Faruk Ahmed, Martin Arjovsky, Vincent Dumoulin, and Aaron C Courville. Improved training of wasserstein gans. *Advances in neural information processing systems*, 30, 2017. [2](#)
- [14] Agrim Gupta, Justin Johnson, Li Fei-Fei, Silvio Savarese, and Alexandre Alahi. Social gan: Socially acceptable trajectories with generative adversarial networks. In *Proceedings of the IEEE conference on computer vision and pattern recognition*, pages 2255–2264, 2018. [1](#), [2](#), [3](#), [4](#), [6](#), [7](#)
- [15] Dirk Helbing and Peter Molnar. Social force model for pedestrian dynamics. *Physical review E*, 51(5):4282, 1995. [1](#)
- [16] Jonathan Ho, Ajay Jain, and Pieter Abbeel. Denoising diffusion probabilistic models. In H. Larochelle, M. Ranzato, R. Hadsell, M.F. Balcan, and H. Lin, editors, *Advances in Neural Information Processing Systems*, volume 33, pages 6840–6851. Curran Associates, Inc., 2020. [2](#), [3](#), [4](#), [8](#)
- [17] Jonathan Ho and Tim Salimans. Classifier-free diffusion guidance. *arXiv preprint arXiv:2207.12598*, 2022. [2](#)
- [18] Sepp Hochreiter and Jürgen Schmidhuber. Long short-term memory. *Neural computation*, 9(8):1735–1780, 1997. [3](#)
- [19] Yingfan Huang, Huikun Bi, Zhaoxin Li, Tianlu Mao, and Zhaoqi Wang. Stgat: Modeling spatial-temporal interactions for human trajectory prediction. In *Proceedings of the IEEE/CVF international conference on computer vision*, pages 6272–6281, 2019. [1](#), [3](#)
- [20] Boris Ivanovic and Marco Pavone. The trajetron: Probabilistic multi-agent trajectory modeling with dynamic spatiotemporal graphs. In *Proceedings of the IEEE/CVF International Conference on Computer Vision*, pages 2375–2384, 2019. [1](#), [2](#), [3](#)
- [21] Animesh Karnewar and Oliver Wang. Msg-gan: Multi-scale gradients for generative adversarial networks. In *Proceedings of the IEEE/CVF conference on computer vision and pattern recognition*, pages 7799–7808, 2020. [2](#)
- [22] Diederik P Kingma and Max Welling. Auto-encoding variational bayes. *arXiv preprint arXiv:1312.6114*, 2013. [4](#)
- [23] Naveen Kodali, Jacob Abernethy, James Hays, and Zsolt Kira. On convergence and stability of gans. *arXiv preprint arXiv:1705.07215*, 2017. [2](#)
- [24] Vineet Kosaraju, Amir Sadeghian, Roberto Martín-Martín, Ian Reid, Hamid Rezaeifighi, and Silvio Savarese. Social-bi-gan: Multimodal trajectory forecasting using bicycle-gan

- and graph attention networks. *Advances in Neural Information Processing Systems*, 32, 2019. 6, 7
- [25] Laura Leal-Taixé, Michele Fenzi, Alina Kuznetsova, Bodo Rosenhahn, and Silvio Savarese. Learning an image-based motion context for multiple people tracking. In *2014 IEEE Conference on Computer Vision and Pattern Recognition, CVPR 2014, Columbus, OH, USA, June 23-28, 2014*, pages 3542–3549. IEEE Computer Society, 2014. 6
 - [26] Namhoon Lee, Wongun Choi, Paul Vernaza, Christopher B Choy, Philip HS Torr, and Manmohan Chandraker. Desire: Distant future prediction in dynamic scenes with interacting agents. In *Proceedings of the IEEE conference on computer vision and pattern recognition*, pages 336–345, 2017. 2, 3
 - [27] Florin Leon and Marius Gavrilescu. A review of tracking and trajectory prediction methods for autonomous driving. *Mathematics*, 9(6), 2021. 1
 - [28] Junwei Liang, Lu Jiang, Juan Carlos Niebles, Alexander G Hauptmann, and Li Fei-Fei. Peeking into the future: Predicting future person activities and locations in videos. In *Proceedings of the IEEE/CVF conference on computer vision and pattern recognition*, pages 5725–5734, 2019. 1, 3
 - [29] Yuejiang Liu, Qi Yan, and Alexandre Alahi. Social nce: Contrastive learning of socially-aware motion representations. In *Proceedings of the IEEE/CVF International Conference on Computer Vision*, pages 15118–15129, 2021. 1, 6, 7
 - [30] Karttikeya Mangalam, Harshayu Girase, Shreyas Agarwal, Kuan-Hui Lee, Ehsan Adeli, Jitendra Malik, and Adrien Gaidon. It is not the journey but the destination: End-point conditioned trajectory prediction. In *Computer Vision—ECCV 2020: 16th European Conference, Glasgow, UK, August 23–28, 2020, Proceedings, Part II 16*, pages 759–776. Springer, 2020. 7
 - [31] Lars Mescheder, Sebastian Nowozin, and Andreas Geiger. Adversarial variational bayes: Unifying variational autoencoders and generative adversarial networks. In *International conference on machine learning*, pages 2391–2400. PMLR, 2017. 2
 - [32] Abdullah Mohamed, Kun Qian, Mohamed Elhoseiny, and Christian Claudel. Social-stgcnn: A social spatio-temporal graph convolutional neural network for human trajectory prediction. In *Proceedings of the IEEE/CVF conference on computer vision and pattern recognition*, pages 14424–14432, 2020. 2, 3, 6, 7
 - [33] Alessio Monti, Angelo Porrello, Simone Calderara, Pasquale Coscia, Lamberto Ballan, and Rita Cucchiara. How many observations are enough? knowledge distillation for trajectory forecasting. In *Proceedings of the IEEE/CVF Conference on Computer Vision and Pattern Recognition*, pages 6553–6562, 2022. 6, 7
 - [34] Stefano Pellegrini, Andreas Ess, Konrad Schindler, and Luc Van Gool. You’ll never walk alone: Modeling social behavior for multi-target tracking. In *IEEE 12th International Conference on Computer Vision, ICCV 2009, Kyoto, Japan, September 27 - October 4, 2009*, pages 261–268. IEEE Computer Society, 2009. 6
 - [35] Alec Radford, Luke Metz, and Soumith Chintala. Unsupervised representation learning with deep convolutional generative adversarial networks. *arXiv preprint arXiv:1511.06434*, 2015. 2
 - [36] Robin Rombach, Andreas Blattmann, Dominik Lorenz, Patrick Esser, and Björn Ommer. High-resolution image synthesis with latent diffusion models. In *Proceedings of the IEEE/CVF Conference on Computer Vision and Pattern Recognition*, pages 10684–10695, 2022. 2
 - [37] Amir Sadeghian, Vineet Kosaraju, Ali Sadeghian, Noriaki Hirose, Hamid Rezaatoughi, and Silvio Savarese. Sophie: An attentive gan for predicting paths compliant to social and physical constraints. In *Proceedings of the IEEE/CVF conference on computer vision and pattern recognition*, pages 1349–1358, 2019. 1, 2, 3, 4, 6, 7
 - [38] Tim Salzmann, Boris Ivanovic, Punarjay Chakravarty, and Marco Pavone. Trajectron++: Dynamically-feasible trajectory forecasting with heterogeneous data. In *Computer Vision—ECCV 2020: 16th European Conference, Glasgow, UK, August 23–28, 2020, Proceedings, Part XVIII 16*, pages 683–700. Springer, 2020. 1, 2, 3, 6, 7
 - [39] Liushuai Shi, Le Wang, Chengjiang Long, Sanping Zhou, Mo Zhou, Zhenxing Niu, and Gang Hua. Sgcn: Sparse graph convolution network for pedestrian trajectory prediction. In *Proceedings of the IEEE/CVF Conference on Computer Vision and Pattern Recognition*, pages 8994–9003, 2021. 3
 - [40] Jascha Sohl-Dickstein, Eric Weiss, Niru Maheswaranathan, and Surya Ganguli. Deep unsupervised learning using nonequilibrium thermodynamics. In *International Conference on Machine Learning*, pages 2256–2265. PMLR, 2015. 2, 5
 - [41] Jiaming Song, Chenlin Meng, and Stefano Ermon. Denoising diffusion implicit models. *arXiv preprint arXiv:2010.02502*, 2020. 2, 5, 6, 7
 - [42] Jianhua Sun, Yuxuan Li, Hao-Shu Fang, and Cewu Lu. Three steps to multimodal trajectory prediction: Modality clustering, classification and synthesis. In *Proceedings of the IEEE/CVF International Conference on Computer Vision*, pages 13250–13259, 2021. 1
 - [43] Jakub Tomczak and Max Welling. Vae with a vampprior. In *International Conference on Artificial Intelligence and Statistics*, pages 1214–1223. PMLR, 2018. 2
 - [44] Ashish Vaswani, Noam Shazeer, Niki Parmar, Jakob Uszkoreit, Llion Jones, Aidan N Gomez, Łukasz Kaiser, and Illia Polosukhin. Attention is all you need. *Advances in neural information processing systems*, 30, 2017. 1, 3, 4
 - [45] Anirudh Vemula, Katharina Muelling, and Jean Oh. Social attention: Modeling attention in human crowds. In *2018 IEEE international Conference on Robotics and Automation (ICRA)*, pages 4601–4607. IEEE, 2018. 1, 3
 - [46] Xing Wei, Haitao Zhang, Shaofan Liu, and Yang Lu. Pedestrian detection in underground mines via parallel feature transfer network. *Pattern Recognit.*, 103:107195, 2020. 1
 - [47] Cunjun Yu, Xiao Ma, Jiawei Ren, Haiyu Zhao, and Shuai Yi. Spatio-temporal graph transformer networks for pedestrian trajectory prediction. In *Computer Vision—ECCV 2020: 16th European Conference, Glasgow, UK, August 23–28, 2020, Proceedings, Part XII 16*, pages 507–523. Springer, 2020. 3, 4, 7

- [48] Ye Yuan, Xinshuo Weng, Yanglan Ou, and Kris M Kitani. Agentformer: Agent-aware transformers for socio-temporal multi-agent forecasting. In *Proceedings of the IEEE/CVF International Conference on Computer Vision*, pages 9813–9823, 2021. 3, 4
- [49] Pu Zhang, Wanli Ouyang, Pengfei Zhang, Jianru Xue, and Nanning Zheng. Sr-lstm: State refinement for lstm towards pedestrian trajectory prediction. In *Proceedings of the IEEE/CVF Conference on Computer Vision and Pattern Recognition*, pages 12085–12094, 2019. 1, 3
- [50] Guoliang Zhao, Yuxun Zhou, Zhanbo Xu, Yadong Zhou, and Jiang Wu. Hierarchical multi-supervision multi-interaction graph attention network for multi-camera pedestrian trajectory prediction. In *Thirty-Sixth AAAI Conference on Artificial Intelligence, AAAI 2022*, pages 4698–4706. AAAI Press, 2022. 1
- [51] Tianyang Zhao, Yifei Xu, Mathew Monfort, Wongun Choi, Chris Baker, Yibiao Zhao, Yizhou Wang, and Ying Nian Wu. Multi-agent tensor fusion for contextual trajectory prediction. In *Proceedings of the IEEE/CVF Conference on Computer Vision and Pattern Recognition*, pages 12126–12134, 2019. 2, 3